

# Generalized spatial differentiation from spin Hall effect of light

Tengfeng Zhu<sup>1†</sup>, Yijie Lou<sup>1†</sup>, Yihan Zhou<sup>1</sup>, Jiahao Zhang<sup>1</sup>, Junyi Huang<sup>1</sup>, Yan Li<sup>3</sup>, Hailu Luo<sup>4</sup>, Shuangchun Wen<sup>4</sup>, Shiyao Zhu<sup>1,2</sup>, Qihuang Gong<sup>3</sup>, Min Qiu<sup>2\*</sup>, Zhichao Ruan<sup>1,2\*</sup>

<sup>1</sup> *Department of Physics, Zhejiang University, Hangzhou 310027, China*

<sup>2</sup> *State Key Laboratory of Modern Optical*

*Instrumentation and College of Optical Engineering,*

*Zhejiang University, Hangzhou 310027, China*

<sup>3</sup> *State Key Laboratory for Mesoscopic Physics and School of Physics,*

*Peking University, Beijing 100871, China*

<sup>4</sup> *Key Laboratory for Micro/Nano Optoelectronic Devices of Ministry of Education,  
School of Physics and Electronics, Hunan University, Changsha 410082, China*

## Abstract

Optics naturally provides us with some powerful mathematical operations. Here we reveal that a single planar interface can compute spatial differentiation to paraxial coherent beams under oblique incidence. We show that intrinsically the spatial differentiation results from the spin Hall effect of light with preparing and postselecting polarization states, in both quantum and classical levels. Since the spin Hall effect of light is a geometrically protected effect, the spatial differentiation generally accompanies light reflection and refraction and occurs at any optical interface, regardless of composition materials and incident angles. We experimentally demonstrate the generality of spatial differentiation and use such an energy-efficient method to perform ultra-fast edge detection. Compared with recent developments in spatial differentiation computing devices from metamaterials and layered structures to surface plasmonic structures and photonic crystal slab/grating, the proposed spin-optical method is generalized with a single optical interface and moreover offers a simple but powerful mechanism to vectorial-field based computation.

---

\* zhichao@zju.edu.cn, minqiu@zju.edu.cn; <sup>†</sup>These authors contributed equally to this work.

## INTRODUCTION

Differentiation is one of the key tenets of mathematics and used in any field of science and engineering. In image processing, spatial differentiation extracts the boundary of objects in an image, which is the essential first step in object detection, feature classification, and data compression [1]. Over the past few years, optical analog computing for spatial differentiation has been of great interest since such a computing enables the massively parallel processing of edge detection to an entire image in a single shot and therefore is much more energy-efficient than standard digital electronic processing [2, 3]. Such computing is in particular attractive for high-throughput operation that arises in applications such as real-time image processing in medical and satellite applications [4, 5]. Traditionally, optical analog computing in the spatial domain uses a bulky system of lenses and filters in linear or nonlinear optics [6, 7]. Recently, there have been theoretical proposals to miniaturize such computing elements down to a single-wavelength or even sub-wavelength scale by using metamaterials/metasurfaces [8–12]. However, the required metamaterial consists of a complex array of meta-atoms, and direct demonstration of image processing is challenging [13, 14]. To relieve fabrication requirement, ones sought to achieve spatial differentiation with layered structures [8, 15–17], surface plasmonic structures [18–20], or photonic crystal slab/grating [21–23]. We experimentally demonstrated edge detection of an image by exciting surface plasmon on a 50nm-thick silver layer [19]. Even so, all of the current proposals can only deal with scalar field image with intensity and phase distribution. Since light also possesses intrinsic polarization degrees of freedom, it is an open issue how to enable vectorial-field optical analog computation.

In this paper, we experimentally demonstrate that generally by analyzing the orthogonal polarization state of a reflected or refracted polarized beam, a single optical planar interface is enough to compute spatial differentiation. Moreover, we show that such a spatial differentiation scheme takes advantage to offer a robust processing on vectorial field images, where two different images can be stored in two different polarization states. Although the resulted spatial differentiation seems counter-intuitive to the common knowledge that no light can pass through two orthogonal polarizers, we show that the spatial differentiation is intrinsically due to the spin Hall effect (SHE) of light: Spin-dependent transverse shift occurs during oblique reflection or refraction on an interface (see the reviews [24–28] including

general SHE of light for spin-dependent transportation phenomena). The spin dependent transverse shift in total reflection case was observed several decades ago [29, 30]. Until recently it was first theoretically studied in the context of geometric Berry phase [31–34] and later as total angular momentum conservation [35, 36]. These theories greatly deepen the understanding of the SHE of light and boost up experimental investigations in different optical systems, from homogeneous isotropic [37–40] to inhomogeneous and anisotropic crystals [41, 42], from multiple-layered dielectric films [43, 44] to metamaterials/metasurfaces [45, 46] and 2D material films [47]. Especially, Hosten and Kwiat identified the connection between optical SHE of photon and classical light and proposed weak measurement method for attaining ultra-high sensitivity to angstrom scale displacements [37].

We note that in contrast to the non-orthogonal operation proposed in weak measurement [37, 39, 40, 42, 48], here the prepared and postselected states are orthogonal in order to realize spatial differentiation, which creates profoundly different output distribution from the original one. To reveal the underlying physics of the spatial differentiation, we experimentally demonstrate it in the simplest case of a single optical interface between two isotropic media. Since the SHE of light is geometrically protected, the spatial differentiation generally occurs on an optical interface regardless of composition materials. Furthermore, since the SHE of light appears in both reflection and refraction [37, 40], below our discussion focuses on the reflection case and the conclusion can be straightforwardly extended to the refraction case.

## MATERIALS AND METHODS

### Spin-optical method to realize spatial differentiation

We show that the SHE of light can lead to spatial differentiation, through a preparation-postselection process to spin states of light, in both quantum and classical levels. To understand the generalized spatial differentiation, we first consider spin-1 photons. The initial state is  $|\Psi_{\text{in}}\rangle = |\varphi_{\text{in}}\rangle |s\rangle$ , where  $|\varphi_{\text{in}}\rangle$  denotes the initial wave function  $|\varphi_{\text{in}}\rangle = \int dy \varphi_{\text{in}}(y) |y\rangle = \int dk_y \tilde{\varphi}_{\text{in}}(k_y) |k_y\rangle$  and  $|s\rangle$  corresponds to the particle's spin state. Due to the coupling between the spin and the transverse momentum, the spin Hall effect represents the wave packet split for the parallel spin state  $|+\rangle$  (left-circularly polarized,  $s = +1$ ) and the

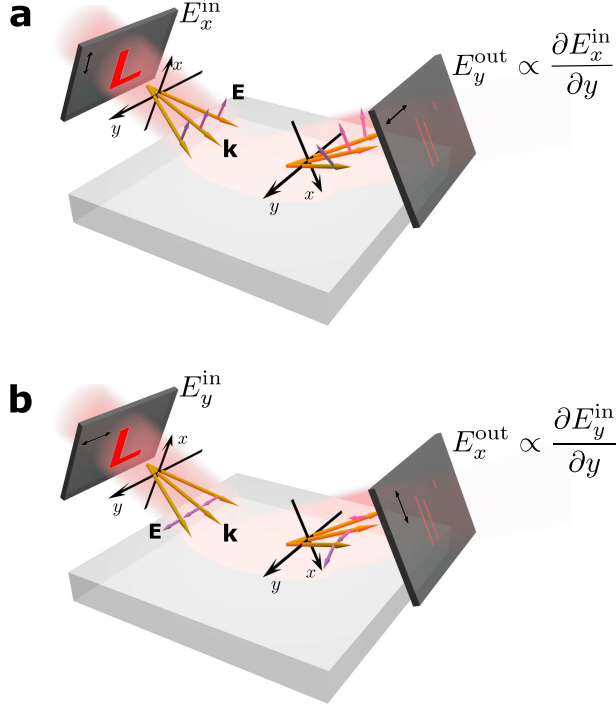


FIG. 1. Schematic of spatial differentiation from the SHE of light on an optical interface between two media. The two orthogonal polarizers (dark grey) enable the preparation-postselection operation with the polarization indicated with double-head arrows: (a) preparing along  $x$  and postselecting along  $y$ , (b) vice versa. As a result, when an incident paraxial beam has an electric field distribution of  $f(x, y)$ , the output field distribution corresponds to  $\partial f / \partial y$ . Here the different rotation of the electric field vectors  $\mathbf{E}$  indicates the different experienced geometric phase of the left- and right-handed circular polarized light for different wavevectors  $\mathbf{k}$  during the light reflection.  $x$  and  $y$  are the beam profile coordinates for the incident and reflected light, which are perpendicular to the beam propagation direction and share the same origin on the interface, and  $x$  is in the incident plane.

antiparallel spin state  $|-\rangle$  (right-circularly polarized,  $s = -1$ ) with shift in opposite direction:  $|\Psi_{\text{out}}\rangle = \hat{U} |\Psi_{\text{in}}\rangle = \int dk_y \tilde{\varphi}_{\text{in}}(k_y) \exp(ik_y \hat{\sigma}_3 \delta) |k_y\rangle |\pm\rangle = \int dy \varphi_{\text{in}}(y \pm \delta) |y\rangle |\pm\rangle$ . Here,  $\hat{U}$  is the evolution operator,  $\hat{\sigma}_3$  is the Pauli matrix along  $z$  and  $\hat{\sigma}_3 |\pm\rangle = \pm |\pm\rangle$ ,  $\exp(ik_y \hat{\sigma}_3 \delta)$  represents a coupling between the spin and the transverse momentum of the spin particles, the wave packets of the parallel and antiparallel spin states shift  $-\delta$  and  $+\delta$ , respectively.

In a special case, when we prepare the initial spin state as  $|u\rangle = \frac{1}{\sqrt{2}}(|+\rangle + |-\rangle)$  and postselect the orthogonal spin state  $|v\rangle = \frac{1}{\sqrt{2}i}(|+\rangle - |-\rangle)$ , the final measured wave function

is left as

$$\begin{aligned}
|\varphi_{\text{out}}\rangle &= \langle v | \hat{U} | \varphi_{\text{in}} \rangle | u \rangle \\
&= \frac{i}{2} \int dk_y \tilde{\varphi}_{\text{in}}(k_y) (e^{ik_y\delta} - e^{-ik_y\delta}) | k_y \rangle \\
&= \frac{i}{2} \int dy [\varphi_{\text{in}}(y + \delta) - \varphi_{\text{in}}(y - \delta)] | y \rangle
\end{aligned} \tag{1}$$

Therefore, if the initial wave function profile is much larger than the shift  $\delta$ , the final output wave function  $|\varphi_{\text{out}}\rangle$  is approximately proportional to the first-order spatial differentiation of the input wave function:

$$|\varphi_{\text{out}}\rangle \simeq i\delta \int dy \xi(y) | y \rangle \tag{2}$$

with  $\xi(y) = d\varphi_{\text{in}}(y)/dy$ . As shown in Eq. (1), the spatial differentiation results from the opposite shifts between the parallel and antiparallel spin states, and the postselected state is orthogonal to the initial one in order to enable destructive interference. Straightforwardly, such a spatial differentiation can also be achieved by preparing the initial spin state  $|v\rangle$  and postselecting the orthogonal spin state  $|u\rangle$ .

The principle of the spatial differentiation from the photonic SHE can be adopted in the classical level with a large number of photons in a quantum-mechanical coherent state, where each photon behaves independently and the light is treated coherently in the paraxial regime. To show the generality of the spatial differentiation, we consider a paraxial beam reflecting on a planar air-glass interface shown in Fig. 1. Suppose the paraxial incident and reflected beams have the vectorial electric fields  $\mathbf{E}_{\text{in}}$  and  $\mathbf{E}_{\text{out}}$  dominating in the transverse direction:  $\mathbf{E}_{\text{in(out)}} = \mathbf{u}_x E_x^{\text{in(out)}}(x, y) + \mathbf{u}_y E_y^{\text{in(out)}}(x, y)$  where  $\mathbf{u}_x$  and  $\mathbf{u}_y$  correspond to the  $x$ - and  $y$ - unit vectors, respectively. Analog to the preparation and postselection operations in quantum level, two polarizers are required to select the incident electric field and analyze the reflected one from the two orthogonal polarizations along  $x$ -direction or  $y$ -direction.

We first consider the incident and reflected electric fields along  $x$  and  $y$ , respectively, as schematically shown in Fig. 1(a):  $\mathbf{E}_{\text{in}} = \mathbf{u}_x E_x^{\text{in}}(x, y)$  and  $\mathbf{E}_{\text{out}} = \mathbf{u}_y E_y^{\text{out}}(x, y)$ . By vectorial spatial Fourier transform, the incident (reflected) beam can be written as the superposition of plane waves,  $E_x^{\text{in}}$  and  $E_y^{\text{out}}$  are written by  $E_{x(y)}^{\text{in(out)}} = \iint \tilde{E}_{x(y)}^{\text{in(out)}}(k_x, k_y) \exp(ik_x x) \exp(ik_y y) dk_x dk_y$ . Due to the continuous condition of the tangential wave vector along the interface, the incident plane wave with  $(k_x, k_y)$  only generates the reflection plane wave with the same  $(k_x, k_y)$ . Therefore, the spatial transform between the incident and reflected electric fields is determined by a spatial spectral transfer function  $H(k_x, k_y) \equiv \tilde{E}_y^{\text{out}}(k_x, k_y)/\tilde{E}_x^{\text{in}}(k_x, k_y)$ . Under

the paraxial approximation [see Supplementary Material for the details], the spatial spectral transfer function is simplified as

$$H = \frac{i(r_s + r_p)}{4}(e^{ik_y\delta} - e^{-ik_y\delta}), \quad (3)$$

where  $r_p$  and  $r_s$  are the Fresnel's reflection coefficients of the  $p$ - and  $s$ -polarizations for the beam incident angle  $\theta_0$ . In Eq. (3),  $\delta$  corresponds to the transverse shift in the SHE of light, which results from the geometric phase experienced by the left- and the right-handed circular polarization elucidated by Bliokh and Bliokh [35, 36, 49]:  $\delta = 2 \cot \theta_0 / k_0$  where  $k_0$  is the wavevector in the incident medium and the factor of 2 is contributed from the twice coordinate basis rotations during the reflection process. Further with the requirement of  $\delta |k_y| \ll 1$ , Eq. (3) is approximated as

$$H \simeq -\frac{\delta(r_s + r_p)}{2}k_y, \quad (4)$$

which is the transfer function of a first-order  $y$ -directional spatial differentiator. Correspondingly, in the spatial domain, the reflected  $E_y^{\text{out}}(x, y)$  field has

$$E_y^{\text{out}} = \frac{i\delta(r_s + r_p)}{2} \frac{\partial E_x^{\text{in}}}{\partial y} \quad (5)$$

Equation (5) shows that analogy to the preparation-postselection scheme in the quantum version, the spatial differentiation can also be realized in the classical electromagnetic field via the spin Hall effect of light, by a single optical interface. Also it is straightforward to show that when switching the preparation-postselection polarizations as preparing with the incident  $y$ -polarized fields  $\mathbf{E}_{\text{in}} = \mathbf{u}_y E_y^{\text{in}}$  and postselecting along  $x$ -direction  $\mathbf{E}_{\text{out}} = \mathbf{u}_x E_x^{\text{out}}$  [Fig. 1(b)], the reflected electric field corresponds to the spatial differentiation of the incident one as

$$E_x^{\text{out}} = \frac{i\delta(r_p + r_s)}{2} \frac{\partial E_y^{\text{in}}}{\partial y} \quad (6)$$

The invariant transverse direction of the spatial differentiation during the switching can be understood since the circular-polarization dependent shifts of the SHE occur in the transverse direction.

## Experimental characterization

To demonstrate the spatial differentiation, we measure the spatial spectral transfer function on an air-glass interface, with the preparation-postselection operation. The experiment

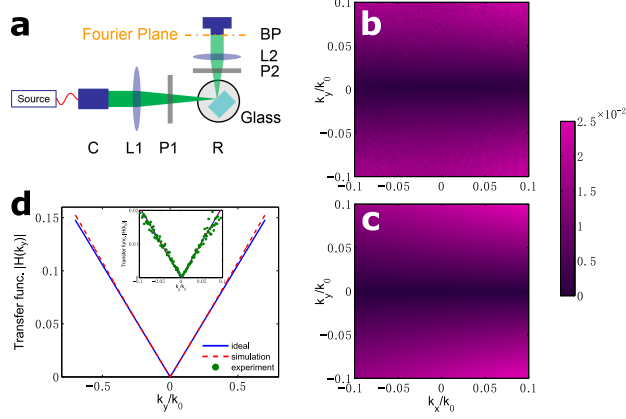


FIG. 2. Measurement of the spatial spectral transfer function on an air-glass interface. (a) Experimental setup: Glass slab (material BK7); R, precision rotator; P1 and P2, polarizers; L1 and L2, lenses with focal lengths 50 and 30 mm, respectively; C, collimator; BP, beam profiler (Ophir SP620). The light source is a green laser (wavelength  $\lambda_0 = 532\text{nm}$ ) and connected to the collimator through a fiber with polarization controller. (b) Measured spatial transfer function spectra. (c) Theoretical results by numerical simulations based on classical electrodynamics. (d) Experimental (dotted line of inset), theoretical (dashed lines) spatial spectral transfer function for  $k_x = 0$ , and the ideal one (solid lines) based on the first-order differentiation of Eq. (4).

setup is schematically shown in Fig. 2(a), where an incident collimated Gaussian laser beam, with the wavelength of 532nm, focuses on a BK7 glass surface with Lens L1, and the refractive index of the BK7 glass is 1.5195. The incident angle is controlled by a precision rotator R. Lens L2 projects the reflected field to the Fourier space at the back focal plane, which is measured by a beam profiler. The polarizer P1 is used to prepare the initial field polarization state, and the other one P2 is to postselect the output polarization state. We note that two polarizers are placed between Lenses L1 and L2 in order to avoid the polarization rotation induced by the geometric phase during light focusing and collimating [50, 51].

The incident spatial spectra are obtained by removing the glass and rotating the reflection path L2 and P2 to the normal incidence. With the polarizer P2 along the same polarization of P1, we measure the incident spatial spectra at the back focal plane of L2. Correspondingly, the spatial spectral transfer function is obtained by normalizing the incident and reflected spectrum data. We measure the incident and the reflected spectra with the beam profiler (Ophir SP620) instead of conventional charge-coupled devices (CCDs) because the CCD

might use gamma correction and cannot accurately measure the field intensity.

## RESULTS AND DISCUSSION

Figure 2(b) shows the measured spatial spectral transfer function for the incident angle  $\theta_0 = 45^\circ$ , where the preparation-postselection operations are with P1 and P2 along  $x$ -direction and  $y$ -direction, respectively. The measured spatial spectral transfer function is shown in the ranges of  $|k_x| < 0.1k_0$  and  $|k_y| < 0.1k_0$ , which are limited by the numerical aperture of the optical system. For comparison, Fig. 2(c) corresponds to the theoretical spatial transfer function by numerical calculation based on classical electrodynamics [see Supplementary Material]. Figs. 2(b) and (c) show that the experimentally measured spectral transfer function coincides with the theoretical one and has the minimum at  $k_y = 0$ . To clearly show the effect of the spatial differentiation, the experimental and numerical transfer functions for  $k_x = 0$  are compared with the ideal first-order differentiation based on Eq. (4). Indeed, the spatial transfer functions agree well and exhibit a linear dependence of  $k_y$  around  $k_y = 0$  [Fig. 2(d)]. More importantly, it shows that the spatial spectrum bandwidth of the  $y$ -direction differentiation is as large as about  $|k_y| < 0.5k_0$ .

We now demonstrate various aspects of the spin-optical spatial differentiation that are important for edge detection. Without any complex structures, a single optical interface greatly simplifies the fabrication process and reduces the influence of fabrication imperfection. Also the differentiation operates on the electric field rather than the intensity. That is, the device can be used to detect an edge either in the phase or the amplitude distribution of the incident field. Furthermore, since the spatial differentiation can process two different polarizations, we can use  $E_x^{\text{in}}$  and  $E_y^{\text{in}}$  for two different images, respectively. Therefore, such a spin-optical method offers a robust computation processing on vectorial fields.

To show such an effect, we use a spatial light modulator (SLM: Holoeye PLUTO-NIR-011) to generate incident fields with amplitude and phase modulations, respectively (see Supplementary Material). Figure 3(a) shows the incident image field consisting of a Chinese character of light generated with amplitude modulation on the field component of  $E_x^{\text{in}}$ , where the inside and the outside of the character have different intensities. Figure 3(b) shows the measured reflected intensity of  $E_y^{\text{out}}$ . It clearly exhibits the outlines of the character with spatial differentiation. Since the differentiation is along the  $y$ -direction, the edges



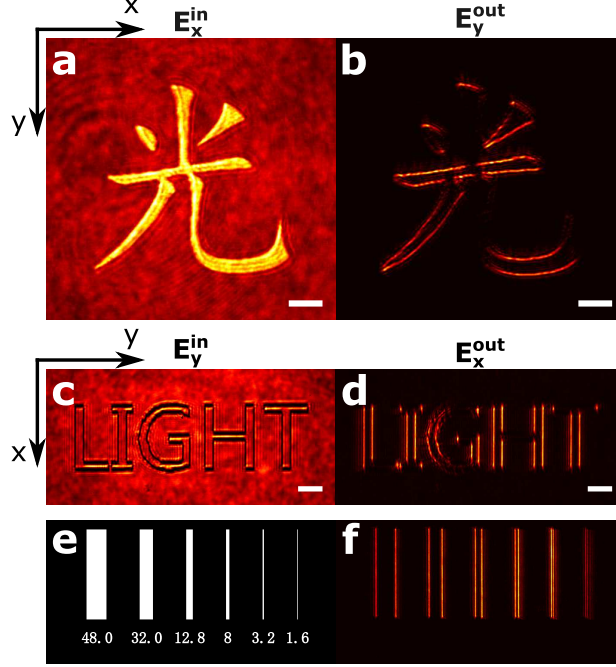


FIG. 3. Edge detection for different images stored in  $E_x^{\text{in}}$  and  $E_y^{\text{in}}$ , respectively, with either amplitude or phase modulation. (a) Incident image consisting of a Chinese character of light with amplitude modulation on  $E_x^{\text{in}}$ , where the inside and the outside of the character have different intensities. (b) Reflected intensity image corresponding to (a) by measuring  $E_y^{\text{out}}$ . (c) Incident image consisting of the LIGHT letters generated with phase modulation on  $E_y^{\text{in}}$ , where the inside and the outside of the letters have different phases but the same intensity. (d) Reflected intensity image corresponding to (c) by measuring  $E_x^{\text{out}}$ . The white bars correspond to the length of 50  $\mu\text{m}$ . (e) Slot test patterns on the SLM with the different phases for the black and the white areas. The widths of the slots list below in  $\mu\text{m}$ . (f) Measured reflected intensity image corresponding to (e).

perpendicular to the  $y$ -direction are most visible. Furthermore as long as the edge is not completely along the  $y$ -direction, it can be detected in the reflected beam. Figure 3(c) shows an incident image field of LIGHT letters generated with phase modulation on the field component of  $E_y^{\text{in}}$ , where the inside and the outside of the letters have the same intensity but with different phases. We note that here we have rotated the incident image to demonstrate that we can detect the vertical edges. Again, the reflected light clearly exhibits only the edges of the letters in the vertical direction by measuring  $E_x^{\text{out}}$  (Fig. 3(d)), which exactly corresponds to spatial differentiation along  $y$ -direction. The differentiator performs spatial differentiation along only a single direction. This directional selectivity feature is very useful

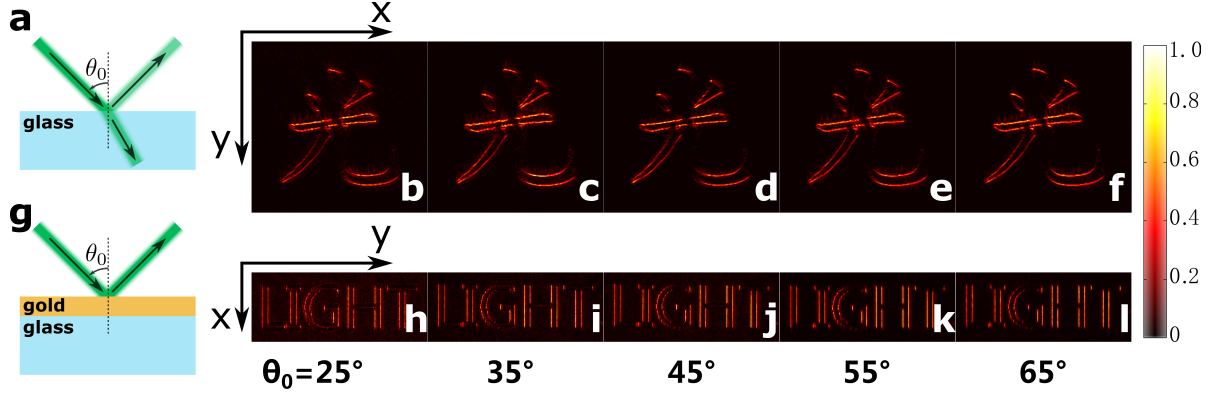


FIG. 4. Edge detection demonstration on different material interfaces and for a variety of incident angles. (a-f) the weak reflection case on the air-glass interface, (g-l) the total reflection case with a planar interface on 210nm-thick gold layer. (a) and (g) are the schematics of the light reflection for two cases, respectively. The spatial differentiation results are shown for the incident images with (b-f) the Chinese character of light and (h-l) the letters of LIGHT. Here the field intensities are normalized with each maximum. The incident angle for each column lists below.

in image processing to determine and classify edge directions [1]. One also can perform differentiation along a perpendicular direction by rotating the beam as demonstrated here.

As shown in Fig. 2(d), since there is a finite spatial bandwidth for the spatial differentiation, it will not be able to resolve two edges that are very close to each other. In order to show the edge detection resolution we generate slot test patterns on the SLM [Fig. 3(e)], and the corresponding reflected intensity is measured and shown in Fig. 3(f). It shows that the minimum separation between the two edges that can be resolved, is about  $3.2 \mu\text{m}$ . The resolution is mainly limited by the small numerical aperture of the image system and can be further improved.

To verify the generality of spin-optical spatial differentiation, we also experimentally demonstrate it for different incident angles and materials. Figures. 4(a-f) show the spatial differentiation results on the air-glass interface for the image with the Chinese character of light, when the incident angle is varied from  $25^\circ$  to  $65^\circ$  with a step of  $10^\circ$ . They clearly demonstrate that the spatial differentiation occurs for all the different incident angles. Moreover, since the SHE of light on the interface is a geometric effect which is independent of material, we also demonstrate the spatial differentiation in the total reflection case on 210nm-thick gold layer. Figures. 4(g-l) show the spatial differentiation results for the image

consisting of the LIGHT letters with different incident angles. Indeed, these results confirm that the spatial differentiation is regardless of the composition materials of the planar interface.

We note that Fig. 4 also shows that the spin-optical method exhibits high signal noise ratio of spatial differentiation. Since the SHE of light vanishes at normal incidence for symmetry reasons, the spatial differentiation signal is decreased with a small value of  $|r_s + r_p|$  when reducing the incident angle [c.f. Eq. (4)]. Here the high signal noise ratio is contributed by the orthogonal preparation-postselection operation strongly reducing background noise. As a result, Fig. 4 clearly presents the edges of the objects for both the weak and total reflection cases, even with a conventional image detector. Also since the original image is still stored in the preparation polarization state and can be retrieved with a polarization beam splitter in the postselection, the spin-optical spatial differentiation enables an energy-efficient and noninvasive measurement which is of great importance to image processing.

## CONCLUSION

We reveal a generalized spatial differentiation based on the SHE of light and experimentally demonstrate it with optical interfaces. The observation of the spin-optical spatial differentiation is dependent on three key elements: oblique incidence, coherent paraxial beam, and polarizer. Since the spatial differentiation results from an interference based on the SHE of light, the light source is required to be coherent. The signal noise ratio of spatial differentiation is mainly determined by the extinction ratio of the polarizers. We note that in some studies on the Brewster effect [52–54], under  $p$ -polarized Gaussian beam illumination, a double-peak reflected beam profile was observed after the  $s$ -polarized analyzer. We believe that these observations were the specific cases of the generalized spatial differentiation discussed here.

Moreover, we show that such a spatial differentiation provides an ultra-fast and energy-efficient method of differentiation measurements to vectorial field images. Since the SHE of light is a non-dispersive effect, in principle, the frequency bandwidth of the spatial differentiation is unlimited and thus the operation is optically fast computed. Furthermore an optical interface can be fabricated in large scale and therefore the space-bandwidth product is sufficient to process large images on a single shot. Due to the general SHE of light

in a variety of optical systems, the proposed vectorial-field based method points a way of spin-optics to information processing and even forwards to the area of electronics.

## DATA AVAILABILITY

The data that support the findings of this study are available from the corresponding author upon reasonable request.

- 
- [1] R. Jain, R. Kasturi, and B. G. Schunck, *Machine vision* (McGraw-Hill, New York, 1995), 1st ed.
  - [2] D. R. Solli and B. Jalali, “Analog optical computing,” *Nature Photonics* **9**, 704–706 (2015).
  - [3] H. J. Caulfield and S. Dolev, “Why future supercomputing requires optics,” *Nature Photonics* **4**, 261 (2010).
  - [4] D. L. Pham, C. Xu, and J. L. Prince, “Current methods in medical image segmentation,” *Annual Review of Biomedical Engineering* **2**, 315–337 (2000).
  - [5] R. J. Holyer and S. H. Peckinpough, “Edge detection applied to satellite imagery of the oceans,” *IEEE Transactions on Geoscience and Remote Sensing* **27**, 46–56 (1989).
  - [6] J. Goodman, *Introduction to Fourier optics* (McGraw-hill, 1996), 2nd ed.
  - [7] X. Qiu, F. Li, W. Zhang, Z. Zhu, and L. Chen, “Spiral phase contrast imaging in nonlinear optics: seeing phase objects using invisible illumination,” *Optica* **5**, 208–212 (2018).
  - [8] A. Silva, F. Monticone, G. Castaldi, V. Galdi, A. Alù, and N. Engheta, “Performing mathematical operations with metamaterials,” *Science* **343**, 160–163 (2014).
  - [9] S. AbdollahRamezani, K. Arik, A. Khavasi, and Z. Kavehvas, “Analog computing using graphene-based metalines,” *Optics Letters* **40**, 5239–5242 (2015).
  - [10] A. Chizari, S. Abdollahramezani, M. V. Jamali, and J. A. Salehi, “Analog optical computing based on a dielectric meta-reflect array,” *Optics Letters* **41**, 3451–3454 (2016).
  - [11] Y. Hwang, T. J. Davis, J. Lin, and X.-C. Yuan, “Plasmonic circuit for second-order spatial differentiation at the subwavelength scale,” *Optics Express* **26**, 7368–7375 (2018).
  - [12] A. Saba, M. R. Tavakol, P. Karimi-Khoozani, and A. Khavasi, “Two dimensional edge detection by guided mode resonant metasurface,” *IEEE Photonics Technology Letters* (2018).

- [13] A. Pors, M. G. Nielsen, and S. I. Bozhevolnyi, “Analog computing using reflective plasmonic metasurfaces,” *Nano Letters* **15**, 791–797 (2014).
- [14] Y. Hwang and T. J. Davis, “Optical metasurfaces for subwavelength difference operations,” *Applied Physics Letters* **109**, 181101 (2016).
- [15] L. L. Doskolovich, D. A. Bykov, E. A. Bezus, and V. A. Soifer, “Spatial differentiation of optical beams using phase-shifted Bragg grating,” *Optics Letters* **39**, 1278–1281 (2014).
- [16] N. V. Golovastikov, D. A. Bykov, L. L. Doskolovich, and E. A. Bezus, “Spatial optical integrator based on phase-shifted Bragg gratings,” *Optics Communications* **338**, 457–460 (2015).
- [17] A. Youssefi, F. Zangeneh-Nejad, S. Abdollahramezani, and A. Khavasi, “Analog computing by Brewster effect,” *Optics Letters* **41**, 3467–3470 (2016).
- [18] Z. Ruan, “Spatial mode control of surface plasmon polariton excitation with gain medium: from spatial differentiator to integrator,” *Optics Letters* **40**, 601–604 (2015).
- [19] T. Zhu, Y. Zhou, Y. Lou, H. Ye, M. Qiu, Z. Ruan, and S. Fan, “Plasmonic computing of spatial differentiation,” *Nature Communications* **8**, 15391 (2017).
- [20] Y. Fang, Y. Lou, and Z. Ruan, “On-grating graphene surface plasmons enabling spatial differentiation in the terahertz region,” *Optics Letters* **42**, 3840–3843 (2017).
- [21] C. Guo, M. Xiao, M. Minkov, Y. Shi, and S. Fan, “Photonic crystal slab laplace operator for image differentiation,” *Optica* **5**, 251–256 (2018).
- [22] D. A. Bykov, L. L. Doskolovich, A. A. Morozov, V. V. Podlipnov, E. A. Bezus, P. Verma, and V. A. Soifer, “First-order optical spatial differentiator based on a guided-mode resonant grating,” *Optics Express* **26**, 10997–11006 (2018).
- [23] Z. Dong, J. Si, X. Yu, and X. Deng, “Optical spatial differentiator based on subwavelength high-contrast gratings,” *Applied Physics Letters* **112**, 181102 (2018).
- [24] K. Y. Bliokh, F. Rodríguez-Fortuño, F. Nori, and A. V. Zayats, “Spin-orbit interactions of light,” *Nature Photonics* **9**, 796–808 (2015).
- [25] A. Aiello, P. Banzer, M. Neugebauer, and G. Leuchs, “From transverse angular momentum to photonic wheels,” *Nature Photonics* **9**, 789 (2015).
- [26] F. Cardano and L. Marrucci, “Spin–orbit photonics,” *Nature Photonics* **9**, 776 (2015).
- [27] S. Xiao, J. Wang, F. Liu, S. Zhang, X. Yin, and J. Li, “Spin-dependent optics with metasurfaces,” *Nanophotonics* **6**, 215–234 (2016).

- [28] X. Ling, X. Zhou, K. Huang, Y. Liu, C.-W. Qiu, H. Luo, and S. Wen, “Recent advances in the spin Hall effect of light,” *Reports on Progress in Physics* **80**, 066401 (2017).
- [29] F. I. Fedorov, “To the theory of total reflection,” *Dokl. Akad. Nauk SSR* **105**, 465–468 (1955).
- [30] C. Imbert, “Calculation and experimental proof of the transverse shift induced by total internal reflection of a circularly polarized light beam,” *Physical Review D* **5**, 789–795 (1972).
- [31] M. Onoda, S. Murakami, and N. Nagaosa, “Hall effect of light,” *Physical Review Letters* **93**, 083901 (2004).
- [32] K. Y. Bliokh and Y. P. Bliokh, “Modified geometrical optics of a smoothly inhomogeneous isotropic medium: the anisotropy, Berry phase, and the optical Magnus effect,” *Physical Review E* **70**, 026605 (2004).
- [33] K. Y. Bliokh, I. V. Shadrivov, and Y. S. Kivshar, “Goos–hänchen and Imbert–fedorov shifts of polarized vortex beams,” *Optics Letters* **34**, 389–391 (2009).
- [34] K. Y. Bliokh and Y. P. Bliokh, “Topological spin transport of photons: the optical Magnus effect and Berry phase,” *Physics Letters A* **333**, 181–186 (2004).
- [35] K. Y. Bliokh and Y. P. Bliokh, “Conservation of angular momentum, transverse shift, and spin Hall effect in reflection and refraction of an electromagnetic wave packet,” *Physical Review Letters* **96**, 073903 (2006).
- [36] K. Y. Bliokh and A. Aiello, “Goos–Hänchen and Imbert–Fedorov beam shifts: an overview,” *Journal of Optics* **15**, 014001 (2013).
- [37] O. Hosten and P. Kwiat, “Observation of the spin Hall effect of light via weak measurements,” *Science* **319**, 787–790 (2008).
- [38] K. Y. Bliokh, A. Niv, V. Kleiner, and E. Hasman, “Geometrodynamics of spinning light,” *Nature Photonics* **2**, 748 (2008).
- [39] Y. Qin, Y. Li, X. Feng, Y.-F. Xiao, H. Yang, and Q. Gong, “Observation of the in-plane spin separation of light,” *Optics Express* **19**, 9636–9645 (2011).
- [40] X. Zhou, X. Ling, Z. Zhang, H. Luo, and S. Wen, “Observation of spin Hall effect in photon tunneling via weak measurements,” *Scientific Reports* **4**, 7388 (2014).
- [41] Y. Qin, Y. Li, X. Feng, Z. Liu, H. He, Y.-F. Xiao, and Q. Gong, “Spin Hall effect of reflected light at the air-uniaxial crystal interface,” *Optics Express* **18**, 16832–16839 (2010).
- [42] K. Y. Bliokh, C. Samlan, C. Prajapati, G. Puentes, N. K. Viswanathan, and F. Nori, “Spin-Hall effect and circular birefringence of a uniaxial crystal plate,” *Optica* **3**, 1039–1047 (2016).

- [43] H. Luo, X. Ling, X. Zhou, W. Shu, S. Wen, and D. Fan, “Enhancing or suppressing the spin Hall effect of light in layered nanostructures,” *Physical Review A* **84**, 033801 (2011).
- [44] B. Wang, Y. Li, M.-M. Pan, J.-L. Ren, Y.-F. Xiao, H. Yang, and Q. Gong, “Spin displacements of a gaussian beam at an air–multilayer-film interface,” *Physical Review A* **88**, 043842 (2013).
- [45] X. Yin, Z. Ye, J. Rho, Y. Wang, and X. Zhang, “Photonic spin Hall effect at metasurfaces,” *Science* **339**, 1405–1407 (2013).
- [46] P. V. Kapitanova, P. Ginzburg, F. J. Rodríguez-Fortuño, D. S. Filonov, P. M. Voroshilov, P. A. Belov, A. N. Poddubny, Y. S. Kivshar, G. A. Wurtz, and A. V. Zayats, “Photonic spin Hall effect in hyperbolic metamaterials for polarization-controlled routing of subwavelength modes,” *Nature Communications* **5**, 3226 (2014).
- [47] X. Zhou, X. Ling, H. Luo, and S. Wen, “Identifying graphene layers via spin Hall effect of light,” *Applied Physics Letters* **101**, 251602 (2012).
- [48] I. Duck, P. M. Stevenson, and E. Sudarshan, “The sense in which a” weak measurement” of a spin-1/2 particle’s spin component yields a value 100,” *Physical Review D* **40**, 2112 (1989).
- [49] K. Y. Bliokh and Y. P. Bliokh, “Polarization, transverse shifts, and angular momentum conservation laws in partial reflection and refraction of an electromagnetic wave packet,” *Physical Review E* **75**, 066609 (2007).
- [50] K. Y. Bliokh, E. A. Ostrovskaya, M. A. Alonso, O. G. Rodríguez-Herrera, D. Lara, and C. Dainty, “Spin-to-orbital angular momentum conversion in focusing, scattering, and imaging systems,” *Optics Express* **19**, 26132–26149 (2011).
- [51] Z. Bomzon and M. Gu, “Space-variant geometrical phases in focused cylindrical light beams,” *Optics Letters* **32**, 3017–3019 (2007).
- [52] Y. Fainman and J. Shamir, “Polarization of nonplanar wave fronts,” *Applied Optics* **23**, 3188–3195 (1984).
- [53] A. Aiello, M. Merano, and J. Woerdman, “Brewster cross polarization,” *Optics Letters* **34**, 1207–1209 (2009).
- [54] M. Merano, A. Aiello, M. Van Exter, and J. Woerdman, “Observing angular deviations in the specular reflection of a light beam,” *Nature Photonics* **3**, 337–340 (2009).

## **ACKNOWLEDGEMENTS**

We acknowledge Prof. Hui Ye for the help to deposit gold layer on the sample. This work was supported by the National Key Research and Development Program of China (No.2017YFA0205700), National Natural Science Foundation of China (NSFC 61675179), and Fundamental Research Funds for the Central Universities (2018QNA3005). M.Q. acknowledges the support by the NSFC (61425023). Y.Li and Q.G. acknowledge the support by the NSFC (11474010, 61590933). H.L. and S.W. acknowledge the support by the NSFC (11474089).

## **AUTHOR CONTRIBUTIONS**

Z.R. conceived the study of spin-optical spatial differentiator and wrote the manuscript with assistance from T.Z.. T.Z., Y.Z., Z.R., and J.H. designed the experiment and built the experimental set-up and carried out the measurement. Y.Lou and J.Z., performed the numerical simulations. Z.R., Y.Li, H.L., S.W., S.Z., Q.G., and M.Q. analyzed the resultant data and commented on the manuscript. Z.R. and M.Q. supervised the project.

## **COMPETING FINANCIAL INTERESTS**

The authors declare no competing financial interests.

## **CORRESPONDING AUTHOR**

Correspondence to Zhichao Ruan or Min Qiu.